

# MAGIC observations of the February 2014 flare of 1ES 1011+496 and measurement of the EBL density

S. Ansoldi<sup>1</sup>, L. A. Antonelli<sup>2</sup>, P. Antoranz<sup>3</sup>, A. Babic<sup>4</sup>, P. Bangale<sup>5</sup>, U. Barres de Almeida<sup>5,25</sup>, J. A. Barrio<sup>6</sup>, J. Becerra González<sup>7,26</sup>, W. Bednarek<sup>8</sup>, E. Bernardini<sup>9</sup>, B. Biasuzzi<sup>1</sup>, A. Biland<sup>10</sup>, O. Blanch<sup>11</sup>, S. Bonnefoy<sup>6</sup>, G. Bonnoli<sup>2</sup>, F. Borraacci<sup>5</sup>, T. Bretz<sup>12,27</sup>, E. Carmona<sup>13</sup>, A. Carosi<sup>2</sup>, R. Clavero, P. Colin<sup>5</sup>, E. Colombo<sup>7</sup>, J. L. Contreras<sup>6</sup>, J. Cortina<sup>11</sup>, S. Covino<sup>2</sup>, P. Da Vela<sup>3</sup>, F. Dazzi<sup>5</sup>, A. De Angelis<sup>1</sup>, G. De Caneva<sup>9</sup>, B. De Lotto<sup>1</sup>, E. de Oña Wilhelmi<sup>14</sup>, C. Delgado Mendez<sup>13</sup>, F. Di Pierro<sup>2</sup>, D. Dominis Prester<sup>4</sup>, D. Dorner<sup>12</sup>, M. Doro<sup>15</sup>, S. Einecke<sup>16</sup>, D. Eisenacher Glawion<sup>12</sup>, D. Elsaesser<sup>12</sup>, A. Fernández-Barral<sup>11</sup>, D. Fidalgo<sup>6</sup>, M. V. Fonseca<sup>6</sup>, L. Font<sup>17</sup>, K. Frantzen<sup>16</sup>, C. Fruck<sup>5</sup>, D. Galindo<sup>18</sup>, R. J. García López<sup>7</sup>, M. Garczarczyk<sup>9</sup>, D. Garrido Terrats<sup>17</sup>, M. Gaug<sup>17</sup>, N. Godinovic<sup>4</sup>, A. González Muñoz<sup>11</sup>, S. R. Gozzini<sup>9</sup>, Y. Hanabata<sup>19</sup>, M. Hayashida<sup>19</sup>, J. Herrera<sup>7</sup>, J. Hose<sup>5</sup>, D. Hrupec<sup>4</sup>, G. Hughes<sup>10</sup>, W. Idec<sup>8</sup>, H. Kellermann<sup>5</sup>, M. L. Knoetig<sup>10</sup>, K. Kodani<sup>19</sup>, Y. Konno<sup>19</sup>, J. Krause<sup>5</sup>, H. Kubo<sup>19</sup>, J. Kushida<sup>19</sup>, A. La Barbera<sup>2</sup>, D. Las<sup>4</sup>, N. Lewandowska<sup>12</sup>, E. Lindfors<sup>20</sup>, S. Lombardi<sup>2</sup>, F. Longo<sup>1</sup>, M. López<sup>6</sup>, R. López-Coto<sup>11</sup>, A. López-Oramas<sup>11</sup>, E. Lorenz<sup>5</sup>, M. Makariev<sup>21</sup>, K. Mallot<sup>9</sup>, G. Maneva<sup>21</sup>, K. Mannheim<sup>12</sup>, L. Maraschi<sup>2</sup>, B. Marcote<sup>18</sup>, M. Mariotti<sup>15</sup>, M. Martínez<sup>11</sup>, D. Mazin<sup>5</sup>, U. Menzel<sup>5</sup>, J. M. Miranda<sup>3</sup>, R. Mirzoyan<sup>5</sup>, A. Moralejo<sup>11</sup>, P. Munar-Adrover<sup>18</sup>, D. Nakajima<sup>19</sup>, V. Neustroev<sup>20</sup>, A. Niedzwiecki<sup>8</sup>, M. Nievas Rosillo<sup>6</sup>, K. Nilsson<sup>20,28</sup>, K. Nishijima<sup>19</sup>, K. Noda<sup>5</sup>, R. Orito<sup>19</sup>, A. Overkemping<sup>16</sup>, S. Paiano<sup>15</sup>, M. Palatiello<sup>1</sup>, D. Paneque<sup>5</sup>, R. Paoletti<sup>3</sup>, J. M. Paredes<sup>18</sup>, X. Paredes-Fortuny<sup>18</sup>, M. Persic<sup>1,29</sup>, J. Poutanen<sup>20</sup>, P. G. Prada Moroni<sup>22</sup>, E. Prandini<sup>10,30</sup>, I. Puljak<sup>4</sup>, R. Reinthal<sup>20</sup>, W. Rhode<sup>16</sup>, M. Ribó<sup>18</sup>, J. Rico<sup>11</sup>, J. Rodriguez Garcia<sup>5</sup>, T. Saito<sup>19</sup>, K. Saito<sup>19</sup>, K. Satalecka<sup>6</sup>, V. Scalzotto<sup>15</sup>, V. Scapin<sup>6</sup>, C. Schultz<sup>15</sup>, T. Schweizer<sup>5</sup>, S. N. Shore<sup>22</sup>, A. Sillanpää<sup>20</sup>, J. Sitarek<sup>11</sup>, I. Snidarcic<sup>4</sup>, D. Sobczynska<sup>8</sup>, A. Stamerra<sup>2</sup>, T. Steinbring<sup>12</sup>, M. Strzys<sup>5</sup>, L. Takalo<sup>20</sup>, H. Takami<sup>19</sup>, F. Tavecchio<sup>2</sup>, P. Temnikov<sup>21</sup>, T. Terzić<sup>4</sup>, D. Tescaro<sup>7</sup>, M. Teshima<sup>5</sup>, J. Thaele<sup>16</sup>, D. F. Torres<sup>23</sup>, T. Toyama<sup>5</sup>, A. Treves<sup>24</sup>, M. Will<sup>7</sup>, R. Zanin<sup>18</sup>, and

(Affiliations can be found after the references)

Received ; accepted

## ABSTRACT

**Context.** In Feb-March 2014, the MAGIC telescopes observed the high-frequency peaked BL Lac 1ES 1011+496 ( $z=0.212$ ) in flaring state at very high energy (VHE,  $E>100\text{GeV}$ ). The flux reached a level more than 10 times higher than any previously recorded bright state of the source.

**Aims.** Description of the characteristics of the flare presenting the light curve and the spectral parameters of the night-wise spectra and the average spectrum of the whole period. From these data we aim at detecting the imprint of the Extragalactic Background Light (EBL) in the VHE spectrum of the source, in order to constrain its intensity in the optical band.

**Methods.** We analyzed the gamma-ray data from the MAGIC telescopes using the standard MAGIC software for the production of the light curve and the spectra. For the measurement of the EBL we implement the method developed by the H.E.S.S. collaboration in which the intrinsic energy spectrum of the source is modeled with a simple function ( $\leq 4$  parameters), and the EBL-induced optical depth is calculated using a template EBL model. The likelihood of the observed spectrum is then maximized, including a scale factor for the EBL opacity among the free parameters.

**Results.** The collected data allowed us to describe the flux changes night by night and also to produce differential energy spectra for all nights of the observed period. The estimated intrinsic spectra of all the nights could be fitted by power-law functions. Evaluating the changes in the fit parameters we concluded that the spectral shape for most of the nights were compatible, regardless of the flux level, which enabled us to produce an average spectrum from which the EBL imprint could be measured with a significance of  $4.6\sigma$  for an opacity normalization factor  $\alpha_0 = 1.07 (-0.13, +0.09)_{\text{stat}} (+0.23, -0.16)_{\text{E, scale}}$ . This measurement constrains the EBL flux density on the wavelength range  $[0.24 \mu\text{m}, 4.25 \mu\text{m}]$  with a peak value at  $1.4 \mu\text{m}$  of  $\lambda F_\lambda = 12.27^{+2.75}_{-1.83} \text{ nW m}^{-2} \text{ sr}^{-1}$  including systematics.

**Key words.** gamma rays – cosmic background radiation – BL Lacertae objects

## 1. Introduction

1ES 1011+496 (RA:  $10^{\text{h}} 15^{\text{m}} 04.1^{\text{s}}$ , DEC:  $+49^{\circ} 26' 01''$ ) is an active galactic nucleus (AGN) classified as a high-frequency BL Lac (HBL), located at redshift  $z=0.212$  (Albert et al. 2007). HBLs have spectral energy distributions (SED) characterized by two

peaks, one located in the UV to soft X-ray band and the second located in the GeV to TeV range, which makes it possible to detect them in very high energy (VHE)  $\gamma$ -rays. 1ES 1011+496 was discovered at VHE by the MAGIC Collaboration in 2007 following an optical high state reported by the Tuorla Blazar Monitoring Programme (Albert et al. 2007). The flux of the

source for the 2007 observations showed no evidence of variability with an emission level of  $F(>200 \text{ GeV}) = (1.58 \pm 0.32) \times 10^{-11} \text{ photons cm}^{-2} \text{ s}^{-1}$ . The observed spectrum at the time of discovery could be approximated by a power-law function with index  $\Gamma = 4.0 \pm 0.5_{\text{stat}} \pm 0.2_{\text{sys}}$  and normalization  $f_0 = (2.0 \pm 0.1) \times 10^{-10} \text{ TeV}^{-1} \text{ cm}^{-2} \text{ s}^{-1}$  at 200 GeV. The systematic uncertainty for the absolute flux level was estimated to be 75%. The estimated intrinsic spectrum assuming the Kneiske et al. (2002) model for the Extragalactic Background Light (EBL) absorption, was a power-law with photon index  $\Gamma_{\text{int}} = 3.3 \pm 0.7_{\text{stat}}$ . Following the discovery, a multi-wavelength (MWL) campaign was organized by MAGIC (Reinthal et al. 2012). For that campaign the source was observed by MAGIC in 25 nights between March and May 2008. The mean integral flux showed a level similar to the one measured during the discovery in 2007 of  $F(>200 \text{ GeV}) = (1.57 \pm 0.30) \times 10^{-11} \text{ photons cm}^{-2} \text{ s}^{-1}$ . The observed  $\gamma$ -ray spectrum could also be fitted with a simple power-law with index  $\Gamma = 3.2 \pm 0.6_{\text{stat}}$  and normalization  $f_0 = (1.6 \pm 0.1) \times 10^{-10} \text{ TeV}^{-1} \text{ cm}^{-2} \text{ s}^{-1}$  at 200 GeV.

A second MWL campaign, also led by MAGIC, observed 1ES 1011+496 in two periods, from 2011 March to April and from 2012 January to May (Ansoldić et al. 2015). No significant variability was measured within the periods of these observations, although the mean integral flux  $F(>200 \text{ GeV}) = (0.79 \pm 0.12_{\text{stat}} \pm 0.05_{\text{sys}}) \times 10^{-11} \text{ photons cm}^{-2} \text{ s}^{-1}$  was lower than in previous observations by MAGIC. The observed spectrum could be fitted with a simple power law with index  $\Gamma = 3.66 \pm 0.22_{\text{stat}} \pm 0.15_{\text{sys}}$  and normalization  $f_0 = (1.33 \pm 0.06_{\text{stat}} \pm 0.20_{\text{sys}}) \times 10^{-10} \text{ TeV}^{-1} \text{ cm}^{-2} \text{ s}^{-1}$  at 200 GeV. Using the EBL model by Domínguez et al. (2011), the de-absorbed differential energy spectrum showed a good agreement with a simple power law function with index  $\Gamma = 2.95 \pm 0.25_{\text{stat}}$  and normalization  $f_0 = (1.87 \pm 0.08_{\text{stat}}) \times 10^{-10} \text{ TeV}^{-1} \text{ cm}^{-2} \text{ s}^{-1}$  at 200 GeV.

Although MAGIC did not measure a significant variability in the 2007, 2008 and 2011/2012 observations, 1ES 1011+496 was still a good candidate to be observed in flaring state. The observation of a bright source at intermediate redshift, like 1ES 1011+496, provides a good opportunity to measure the impact of the EBL on the propagation of gamma rays over cosmological distances. The EBL is the diffuse radiation that came from the contributions of all the light emitted by stars in the UV-optical and near infrared (NIR) bands and the infrared (IR) radiation emitted by dust after absorbing the starlight, plus a small contribution from active galactic nuclei. Very high-energy (VHE)  $\gamma$ -rays from extragalactic sources interact with the EBL in the optical and NIR bands, producing electron-positron pairs, which causes an attenuation of the VHE photon flux measured at Earth (Gould & Schröder 1967).

Measuring directly the EBL is a challenging task due to the intense foreground light from interplanetary dust. For the optical band strict lower limits to the EBL have been derived from galaxy counts (Madau & Pozzetti 2000; Fazio et al. 2004; Dole et al. 2006). At NIR wavelengths, one way to access to the EBL is by large-scale anisotropy measurements (e.g. Cooray et al. 2004; Fernandez et al. 2010; Zemcov et al. 2014). Making reasonable assumptions on the intrinsic VHE spectra (e.g. limited hardness) of extragalactic sources, upper limits to the EBL density can be derived (e.g. Stecker & de Jager 1996; Aharonian et al. 2006; Mazin & Raue 2007). More recently, extrapolations of data from the Fermi Large Area Telescope have been used to set constraints to the intrinsic VHE spectra of distant sources, which, in combination with Imaging Atmospheric Cherenkov Telescopes (IACT) observations of the same objects, have also

provided upper limits to the EBL density (Georganopoulos et al. 2010; Orr et al. 2011; Meyer et al. 2012).

The Fermi collaboration employed a different technique to actually measure the EBL density using a likelihood ratio test on LAT data from a number of extragalactic sources (Ackermann et al. 2012). Spectral energy distributions from 150 BL Lacs in the redshift range 0.03 - 1.6 were modeled as log parabolae in the optical-thin regime ( $E < 25 \text{ GeV}$ ), then extrapolated to higher energies and compared with the actually observed photon fluxes. A likelihood ratio test was used to determine the best-fit scaling factor for the optical depth  $\tau(E, z)$  according to a given EBL model, hence providing a measurement of the EBL density relative to the model prediction. Several EBL models were tested using this technique (e.g. Stecker et al. 2006; Finke et al. 2010), including the most widely and recently used by IACTs by Franceschini et al. (2008); Domínguez et al. (2011). They obtained a measurement of the UV component of the EBL of  $3 \pm 1 \text{ nW m}^{-2} \text{ sr}^{-1}$  at  $z \approx 1$ .

The H.E.S.S. collaboration used a similar likelihood ratio test to measure the EBL taking advantage of their observations of distant sources at VHE. The EBL absorption at VHE is expected to leave a imprint in the observed spectra, coming from a distinctive feature (an inflection point in the log flux - log E representation) between  $\sim 100 \text{ GeV}$  and  $\sim 5\text{-}10 \text{ TeV}$ , a region observable by IACTs. The H.E.S.S. collaboration modeled the intrinsic spectra of several AGNs using simple functions (up to 4 parameters), then applied a flux suppression factor  $\exp(-\alpha \times \tau(E, z))$ , where  $\tau$  is the optical depth according to a given EBL model and  $\alpha$  a scaling factor. A scan over  $\alpha$  was performed to achieve the best fit to the observed VHE spectra (Abramowski et al. 2013). The no-EBL hypothesis,  $\alpha = 0$ , was excluded at the  $8.8\sigma$  level, and the EBL flux density was constrained in the wavelength range between  $0.30 \mu\text{m}$  and  $17 \mu\text{m}$  (optical to NIR) with a peak value of  $15 \pm 2_{\text{stat}} \pm 3_{\text{sys}} \text{ nW m}^{-2} \text{ sr}^{-1}$  at  $1.4 \mu\text{m}$ .

In Domínguez et al. (2013), data from 1ES 1011+496 was used as part of a data set from several AGNs to measure the cosmic  $\gamma$ -ray horizon (CGRH). The CGRH is, by definition, the energy at which the optical depth of the photon-photon pair production becomes unity as function of redshift. Using MWL data, Domínguez et al. modeled the SED of each source, including 1ES 1011+496, doing a prediction for the VHE band, and then made a comparison with the observed VHE data. In the case of 1ES 1011+496, they compared their modeled SED with the VHE data taken in 2007 by MAGIC. Their prediction was below the observed VHE data, which led to no optical-depth information. A similar approach was presented by Mankuzhiyil et al. (2010), where they modeled the SED of PKS 2155-304 making a prediction for the VHE band and compared it to the observed data to give attenuation limits.

In this paper we present the analysis of the extraordinary flare of 1ES 1011+496 in 2014 February-March observed by the MAGIC telescopes, and apply a technique based on Abramowski et al. (2013) for measuring the EBL. The observations and the data reduction are described in Sect. 2, the results in Sect. 3, the procedure for measuring the EBL in Sect. 4. and the results of the EBL measurement are discussed in Sect. 5.

## 2. Observations & Analysis

MAGIC is a stereoscopic system of two 17 m diameter IACT situated at the Roque de los Muchachos, in the Canary island of La Palma ( $28.75^\circ\text{N}$ ,  $17.86^\circ\text{W}$ ) at a height of 2200 m above sea level. Since the end of 2009, it has been working in stereoscopic mode with a trigger threshold of  $\sim 50 \text{ GeV}$ .

During 2011 and 2012, MAGIC underwent a major upgrade in two stages. First, in summer 2011, the readout electronics of the telescopes were upgraded from multiplexed FADCs in MAGIC-I and Domino Ring Sampler version 2 in MAGIC-II, to Domino Ring Sampler version 4 in both telescopes (Sitarek et al. 2013). Then in summer 2013, the camera of MAGIC-I was replaced by a uniformly pixelized one, as the camera of MAGIC-II (Mazin et al. 2013). With the new system the integral sensitivity achieved is of  $(0.66 \pm 0.03)\%$  of the Crab nebula flux above 220 GeV in 50 hours at low zenith angles (MAGIC Collaboration et al. 2014).

On February 5th 2014, VERITAS issued an alert for the flaring state of 1ES 1011+496. MAGIC performed target of opportunity (ToO) observations for 17 nights during February-March 2014 in the zenith range of  $20^\circ$ – $56^\circ$ . After the quality cuts, 11.8 hrs of good data were used for further analysis. The data were taken in the so-called wobble-mode where the pointing direction alternates between four sky positions at  $0.4^\circ$  away from the source (Fomin et al. 1994). The four wobble positions are used in order to decrease the systematic uncertainties in the background estimation.

The data were analyzed using the standard routines in the MAGIC software package for stereoscopic analysis, MARS (Zanin et al. 2013). For every event we calculated the image size (number of photoelectrons) and the angular distance  $\theta$  between the source position and the reconstructed  $\gamma$ -ray arrival direction. The arrival direction was estimated combining the information from each telescope using the Disp method (Fomin et al. 1994; Zanin et al. 2013). The separation between gamma and hadronic events was performed using a random forest algorithm (Albert et al. 2008). Energy look-up tables generated with Monte Carlo simulations were used to estimate the energy of each event.

### 3. Results

The applied cuts and the zenith angle of the observations result in 3219 events above the energy threshold of 63 GeV in the distribution of the squared angular distance  $\theta^2$  between the reconstructed event direction and the nominal position of 1ES 1011+496. To evaluate the residual background of the observation, three control regions with the same gamma-ray acceptance as the ON region were used to estimate the residual background recorded together with the signal. The source was detected with a significance of  $\sim 75\sigma$ , calculated according to Li & Ma (1983, eq. 17).

Fig. 1 shows the night by night  $\gamma$ -ray light curve for energies  $E > 200$  GeV between February 6th and March 7th 2014. The emission in this period had a high night-to-night variability, reaching a maximum of  $(2.32 \pm 0.14) \times 10^{-10} \text{ cm}^{-2} \text{ s}^{-1}$ ,  $\sim 14$  times the mean integral flux measured by MAGIC in 2007 and 2008 for 1ES 1011+496 (Albert et al. 2007; Reinthal et al. 2012) and  $\sim 29$  times the mean integral flux from the observation in 2011–2012 (Ansoldi et al. 2015). For most of the nights the exposure time was  $\sim 40$  minutes, only for two nights (February 8th and 9th) the observations were extended to  $\sim 2$  hours. No significant intra-night variability was observed at the time scale of  $\sim 20$  minutes.

The averaged observed spectrum for the whole data set was fitted to a log-parabola function (see Fig. 2):

$$\frac{dF}{dE} = f_0 \left( \frac{E}{E_0} \right)^{-\Gamma - \beta \log(E/E_0)} \quad (1)$$

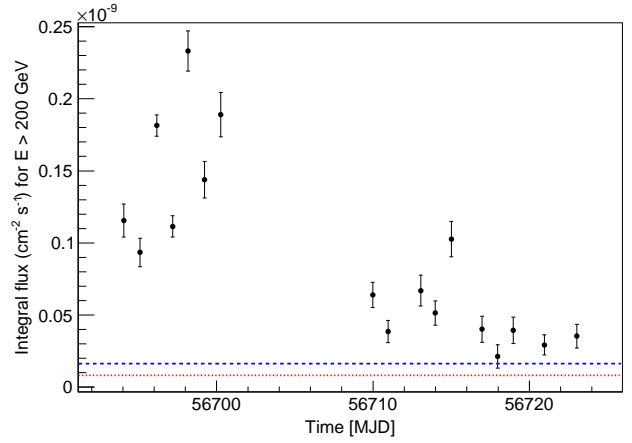


**Fig. 1.** 1ES 1011+496 light curve between February 6th and March 7th 2014 above an energy threshold of 200 GeV with a night-wise binning. The blue dashed line indicates the mean integral for the MAGIC observations of 2007 and the blue dotted line the MWL campaign between 2011 and 2012.

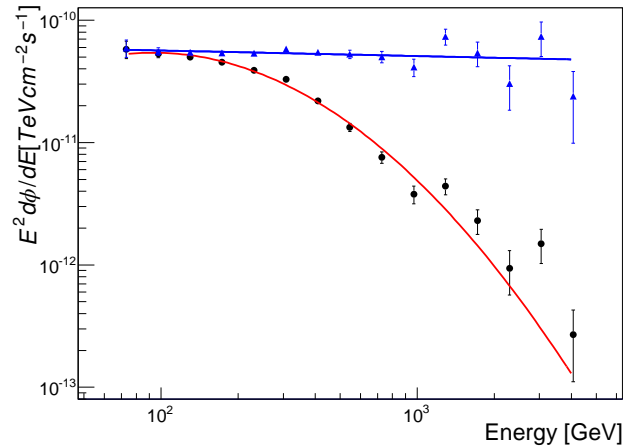


**Fig. 2.** Spectral energy distribution (SED) of 1ES 1011+496 for the 17 nights of observations between February 6th and March 7th 2014. The black dots are the observed data and the blue triangles are the data after EBL de-absorption. The red line indicate the fit to a log-parabola function of the observed SED whereas the blue line indicate the fit to a power-law function of the de-absorbed SED.

with a probability of 0.002 and  $\chi^2 = 30.7/12$ . The photon index is  $\Gamma = 2.84 \pm 0.03$ , curvature index  $\beta = 0.99 \pm 0.05$  and normalization factor at  $E_0 = 250$  GeV  $f_0 = (3.58 \pm 0.10) \times 10^{-11} \text{ cm}^{-2} \text{ s}^{-1} \text{ TeV}^{-1}$ . The de-absorbed spectrum using the EBL model by Domínguez et al. (2011) can be fitted with a simple power-law function with a photon index  $\Gamma = 2.05 \pm 0.03$  and normalization factor at 250 GeV  $f_0 = (5.42 \pm 0.10) \times 10^{-11} \text{ cm}^{-2} \text{ s}^{-1} \text{ TeV}^{-1}$ .

From the light curve is clear that the flux was changing significantly from night to night. For the description of the night-wise spectra we de-absorbed the spectrum of each night with the EBL model by Domínguez et al. (2011). These spectra could be fitted with simple power-law functions. The evolution of the photon index of the fits can be seen in Fig. 3. The energy range for each fit was set to the energy range of each night spectra. Also for each night the correlation energy was computed. For the first seven nights of the observed period, with exception of the night of February 8th, all photon indices are compatible with

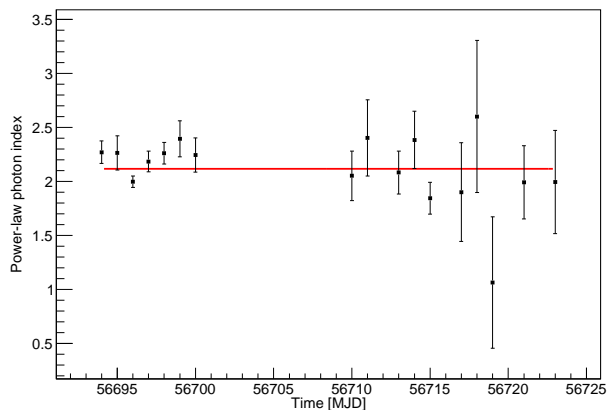


**Fig. 3.** Evolution of the photon index from power-law fits to the de-absorbed night-wise spectra of 1ES 1011+496 between February 6th and March 7th 2014. The error bars are the parameter uncertainties from the fits. The red line represents the fit to a simple line, for which the probability is 10%. If the night of February 8th (third point from the left) is not included in the fit, the probability is almost 50%.

each other within errors. In the latter part of the observed period, the activity of the source was lower and it was observed in shorter periods of times each night compared with the first days, resulting in bigger uncertainties for the fits.

#### 4. EBL measurement

We follow the procedure described in Abramowski et al. (2013) for the likelihood ratio test. The absorption of the EBL is described as  $e^{-\alpha\tau(E,z)}$  where  $\tau(E,z)$  is the optical depth predicted by the model, which depends on the energy  $E$  of the  $\gamma$ -rays and the redshift  $z$  of the source. With the optical depth scaled by a factor  $\alpha$ , the observed spectrum is determined as:

$$(dF/dE)_{obs} = (dF/dE)_{int} \times \exp(-\alpha \times \tau(E, z)) \quad (2)$$

where  $(dF/dE)_{int}$  is the intrinsic spectrum of the source. The emission of HBLs, like 1ES 1011+496, is often well described by basic synchrotron self-Compton (SSC) models (e.g. Tavecchio et al. 1998). A population of electrons are Fermi-accelerated to a ultrarelativistic energies with a resulting power-law spectrum with index  $\Gamma_e$  of about 2. The high energy electrons are cooled faster than the low energy ones, resulting in a steeper  $\Gamma_e$ . These electrons produce synchrotron radiation with a photon index  $\Gamma = \frac{\Gamma_e+1}{2} = 1.5$ . In the Thomson regime the energy spectrum index of the inverse-Compton scattered photons is approximately the same as the synchrotron energy spectrum, whereas in the Klein-Nishima regime, the resulting photon index is even larger. These arguments put serious constraints to the photon index of the energy spectrum of VHE photons. Additionally, in most of the SSC models, the emission is assumed to be originated in a single compact region, which results in a smooth, convex spectral energy distribution with two peaks. This two-peak shape could be modified in a multizone model, where the emission is a superposition of several one-zone emission regions.

For the modeling of the intrinsic source spectrum we have used the same functions as in Mazin & Raue (2007) and Abramowski et al. (2013): power-law (PWL), log-parabola (LP), power-law with exponential cut-off (EPWL), log-parabola with exponential cut-off (ELP) and power-law with superexponential cut-off (SEPWL). We have added an additional constraint,

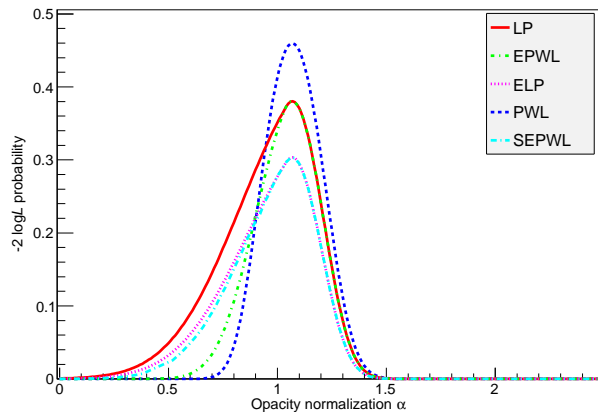


**Fig. 4.**  $-2 \log \mathcal{L}$  probabilities distributions for the average spectrum of the Feb-March flare of 1ES 1011+496 for the 4 models tested. PWL in blue (dashed line), LP in red (solid line), EPWL in green (dash-dot line), ELP in pink (dotted line) and SEPWL in light blue (long dash-dot line).

though, namely that the shapes cannot be concave, i.e. the hardness of the spectrum cannot increase with energy, as this is not expected in emission models, nor has it been observed in any BL Lac in the optically-thin regime.

To search for the imprint of the EBL on the observed spectrum, a scan over  $\alpha$  was computed, varying the value from 0 to 2.5. In each step of the scan, the model for the intrinsic spectrum is modified using the EBL model by Domínguez et al. (2011), with scaled optical depth using the expression (2) and then is passed through the response of the MAGIC telescopes (accounting for the effective area of the system, energy reconstruction, observation time). Then the Poissonian likelihood of the actual observation (the post-cuts number of recorded events vs  $E_{est}$ , in both the ON and OFF regions) is computed, after maximizing it in a parameter space which includes, besides the intrinsic spectral parameters, the Poisson parameters of the background in each bin of  $E_{est}$ . The maximum likelihood is thus obtained for each value of alpha. This likelihood will show a maximum at a value  $\alpha = \alpha_0$ , indicating the EBL opacity scaling which achieves a best fit to the data. A likelihood ratio test is then performed to compare the no-EBL hypothesis ( $\alpha = 0$ ) with the best-fit EBL hypothesis ( $\alpha = \alpha_0$ ). The test statistics  $TS = 2 \log(\mathcal{L}(\alpha = \alpha_0)/\mathcal{L}(\alpha = 0))$  where  $\mathcal{L}$  is the likelihood, according to Wilks theorem, will asymptotically follow a  $\chi^2$  distribution with one degree of freedom (since the two hypothesis differ by just one free parameter,  $\alpha$ ).

To apply the TS we decided to use an average spectrum, so the event statistic are large and the Poissonian likelihood behaves close to its asymptotic limits. Despite changing the flux level, the EBL determination method should work properly as long as the average intrinsic spectrum in the observation period can be described with one of the tested parameterizations. This would of course be the case if the spectral shape is stable, or changes moderately. A varying spectral shape would in any case need quite some fine tuning to reproduce, in the average spectrum, a feature like the one expected to be induced by the EBL. A simple way to check the stability of the spectral shape is fitting the points on the Fig. 3 to a simple line. The  $\chi^2$  of this fit is 23.5/16 and the probability is 10%.

Fig. 4 shows the  $-2 \log \mathcal{L}$  probabilities for the five tested models. The model that gives the highest probability in the

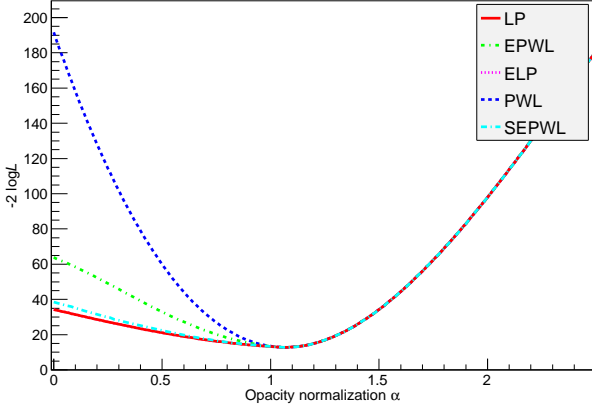


**Fig. 5.**  $-2 \log \mathcal{L}$  distributions for the average spectrum of the Feb-March flare of 1ES 1011+496 for the 5 models tested. PWL in blue (dashed line), LP in red (solid line), EPWL in green (dot-dash line) and ELP in pink (dotted line) and SEPWL in light blue (long dash-dot line). The LP red line is overlapping ELP pink line. Notice how all curves converge after reaching the minimum.

scanned range of  $\alpha$  is the PWL. However, the selection of a PWL as model for the intrinsic spectrum, following the approach of Abramowski et al. (2013) is rather questionable, since would not allow any intrinsic spectral curvature, meaning that all curvature in the observed spectrum must come from the EBL absorption. Such strong and unrealistic assumption would result in an EBL “detection” at the  $\sim 13$  sigma level. We prefer to adopt a more conservative approach, choosing the second-best function, the log-parabola, which is the one providing the best fit for the no-EBL hypothesis. Note however that at the best-fit  $\alpha$ , all the tested functions become simple power-laws, hence the fit probabilities at the peak depend only on the number of free parameters.

Going deeper in the behavior of the fits for the five models, it can be seen in the Fig. 5 that after reaching the minimum, the  $-2 \log \mathcal{L}$  are identical for all models. This happens because of the convexity restriction imposed to the functions: in the LP the curvature  $\beta$  can take only positive values and for the EPWL, ELP and SEPWL the cut-off energies can only be positive. After reaching the point where the EBL de-absorption result in a straight power-law intrinsic spectrum, all three functions converge, and the de-absorbed spectra become more and more concave as  $\alpha$  increases. The shape of the spectrum observed by MAGIC is thus very convenient for setting upper bounds to the EBL density, under the adopted assumption that concave spectra are “unphysical”.

Given the arguments in the previous lines, we take the LP as our model for the intrinsic spectrum. For the data sample from the 2014 February-March flare of 1ES 1011+496, the test statistics has a maximum of  $TS = 21.5$  at  $\alpha_0 = 1.07^{+0.09}_{-0.13}$ . This means that the EBL optical depth from the model of Domínguez et al. (2011) scaled by the normalization factor  $\alpha_0$  is preferred over the null EBL hypothesis with a significance of  $4.6\sigma$ . Choosing the EBL model used by Abramowski et al. (2013) does not alter the result beyond the statistical uncertainty. For the EBL model by Franceschini et al. (2008), the test statistic using the LP as model for the intrinsic spectrum has a maximum of  $TS=20.6$  at  $\alpha_0 = 1.14^{+0.09}_{-0.14}$ .

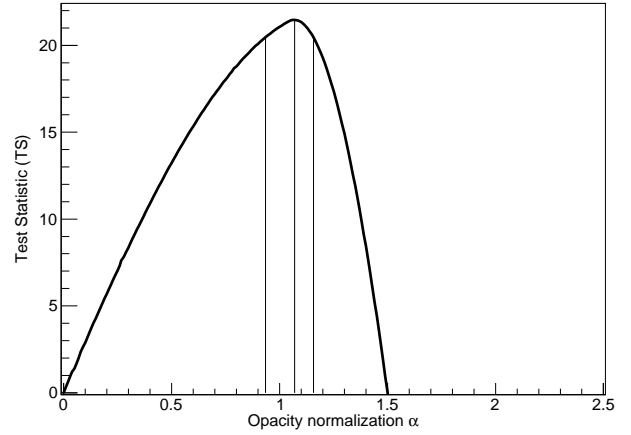


**Fig. 6.** Test statistics distribution for the data sample for the 2014 Feb-March flare of 1ES 1011+496. The vertical lines mark the maximum and the uncertainty corresponding to  $1\sigma$ .

## 5. Systematic uncertainties

The MAGIC telescopes has a systematic uncertainty in the absolute energy scale of 15% (MAGIC Collaboration et al. 2014). The main source of this uncertainty is the imprecise knowledge of the atmospheric transmission. In order to assess how this uncertainty affects the EBL measurement, the calibration constants used to convert the pixel-wise digitized signals into photoelectrons were multiplied by a scaling factor (the same for both telescopes) spanning the range -15% to +15% in steps of 5%. For each of the scaling factors the data were processed in an identical manner through the full analysis chain, starting from the image cleaning, and using in all cases the standard MAGIC MC for this observation period. In this way we try to assess the effect of a potential miscalibration between the data and the MC simulation.

For all scaled data samples,  $-2 \log L$  profiles for  $\alpha$  between 0 and 2.5 were computed. Comparing the profiles, we looked for the one has the shallowest shape around the minimum  $-2 \log L$ , that is, the one that has the maximum statistical uncertainty around  $\alpha_{E, \text{scale}}$ . Since this statistical uncertainty for this particular value of  $\alpha_{E, \text{scale}}$  arose from changing the energy scale, we can interpret it as a systematic uncertainty. Including this uncertainty, the measurement for the opacity normalization factor is  $\alpha_0 = 1.07 (-0.13, +0.09)_{\text{stat}} (+0.23, -0.16)_{E, \text{scale}}$ .

## 6. Discussion

The relation of the  $\gamma$ -ray of energy  $E_\gamma$  from the source and the EBL wavelength at the peak of the cross section for the photon-photon interaction is given by:

$$\lambda_{\text{EBL}}(\mu\text{m}) = 1.187 \times E_\gamma(\text{TeV}) \times (1+z)^2 \quad (3)$$

Where  $z$  is equal or less than the redshift of the source. The energy range used for our calculations was between 0.06 and 3.5 TeV. However, the measurement of the EBL following the method from Abramowski et al. (2013) is based in the fact that after de-absorbing the EBL effect, with the right normalization, the feature between  $\sim 100$  GeV and  $\sim 5$ -10 TeV is suppressed. In Fig. 7 we show a comparison between two cases where the residuals were computed (ratio between the observed events and the expected events from the model). The plot on the left shows



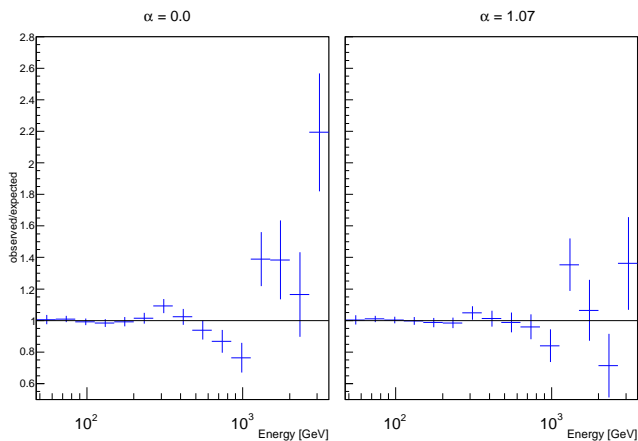


**Fig. 7.** Ratio between the observed events and the expected events from the model of the intrinsic spectrum for two normalization values of the EBL optical depth,  $\alpha = 0$  to the left and  $\alpha = 1.07$  to the right, which corresponds to the normalization where the maximum TS was found. In both plots the line corresponding to a ratio=1 is shown.

the residuals for the null EBL hypothesis  $\alpha = 0$ , while the right pad shows the same plot for the case of the best fit EBL scaling  $\alpha = 1.07$ . The differences start to become evident after 200 GeV, a region where the EBL introduces a feature (an inflection point) that cannot be fitted by the log-parabola. Since it is the feature what drives the TS value on which the EBL measurement is based we decided to take the energy range between 0.2 to 3.5 TeV to calculate the corresponding EBL wavelength range for which our measurement is valid.

The energy range has to take into account the redshift dependency in Eq. (3) since the interaction of the  $\gamma$ -ray and the EBL photon can happen in any point between the Earth and the source. The range is between  $[(1+z)^2 E_{min}, E_{max}]$ , corresponding to a wavelength range of the EBL where the interaction with the  $\gamma$ -ray can take place along the entire path between the source and the Earth. In Fig. 8 we show the contours from the statistical + systematic uncertainty of the EBL flux density, derived scaling up the EBL template model by Domínguez et al. (2011) at redshift  $z = 0$ . The wavelength coverage is in the so-called cosmic optical background (COB) part of the EBL, where we found the peak flux density  $\lambda F_\lambda = 12.27^{+2.75}_{-1.83}$  nW m<sup>-2</sup> sr<sup>-1</sup> at 1.4  $\mu$ m, systematics included.

## 7. Conclusions

We have reported the observation of the extraordinary outburst from 1ES 1011+496 observed by MAGIC from February 6th to March 7th 2014 where the flux reached a level  $\sim 14$  times the observed flux at the time of the discovery of the source in 2007. Although the source showed a high flux variability during the observed period, most of the nights showed a compatible spectral shape, that allowed us to produce and average spectrum that could be fitted with a smooth simple function as the LP, enabling the measurement of the EBL imprint. The EBL was detected with a significance of  $4.5\sigma$  in a EBL wavelength range covering most of the COB region, with a peak of  $\lambda F_\lambda = 12.27^{+2.75}_{-1.83}$  nW m<sup>-2</sup> sr<sup>-1</sup> at 1.4  $\mu$ m, systematics included. This result is compatible with the measurement from Abramowski et al. (2013) with the novelty that we observed to a farther distance of redshift  $z=0.212$ .

*Acknowledgements.*

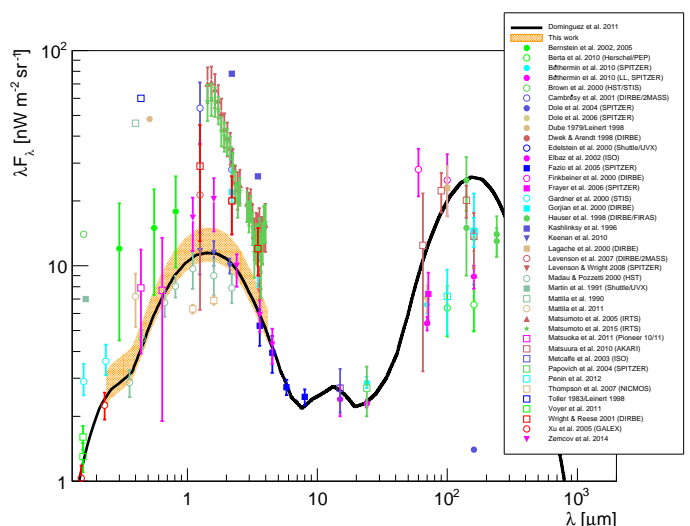


**Fig. 8.** Extragalactic background light intensity versus wavelength at  $z = 0$ . The solid black line is the EBL template model (Domínguez et al. 2011) that we used for our calculations. The orange shaded area spans the wavelength range for which our measurement is valid, scaled from the EBL template. The width of the shaded area includes the statistical and systematic uncertainties. As a comparison we include EBL measurements by Berta et al. (2010), Béthermin et al. (2010), Brown et al. (2000), Cambrésy et al. (2001), Dole et al. (2004), Dwek & Arendt (1998), Elbaz et al. (2002), Finkbeiner et al. (2000), Frayer et al. (2006), Gardner et al. (2000), Gorjian et al. (2000), Hauser et al. (1998), Kashlinsky et al. (1996), Keenan et al. (2010), Lagache et al. (2000), Levenson et al. (2007), Levenson & Wright (2008), Matsumoto et al. (2005), Matsumoto et al. (2015), Matsuoka et al. (2011), Metcalfe et al. (2003), Papovich et al. (2004), Pénin et al. (2012), Thompson et al. (2007), Voyer et al. (2011) and Xu et al. (2005).

## References

- Abramowski, A., Acero, F., & et al. 2013, A&A, 550, A4
- Ackermann, M., Ajello, M., Allafort, A., Schady, P., & et al. 2012, Science, 338, 1190
- Aharonian, F., Akhperjanian, A. G., Bazer-Bachi, A. R., & et al. 2006, Nature, 440, 1018
- Albert, J., Aliu, E., Anderhub, H., Antoranz, P., & et al. 2007, ApJ, 667, L21
- Albert, J., Aliu, E., Anderhub, H., Antoranz, P., & et al. 2008, NIMPR, 588, 424
- Ansoldi, S., Antonelli, A., Antoranz, P., & et al. 2015, In preparation
- Berta, S., Magnelli, B., Lutz, D., et al. 2010, A&A, 518, L30
- Béthermin, M., Dole, H., Beelen, A., & Aussel, H. 2010, A&A, 512, A78
- Brown, T. M., Kimble, R. A., Ferguson, H. C., et al. 2000, AJ, 120, 1153
- Cambrésy, L., Reach, W. T., Beichman, C. A., & Jarrett, T. H. 2001, ApJ, 555, 563
- Cooray, A., Bock, J. J., Keatin, B., Lange, A. E., & Matsumoto, T. 2004, ApJ, 606, 611
- Dole, H., Lagache, G., Puget, J.-L., et al. 2006, A&A, 451, 417
- Dole, H., Rieke, G. H., Lagache, G., et al. 2004, ApJS, 154, 93
- Domínguez, A., Finke, J. D., Prada, F., et al. 2013, ApJ, 770, 77
- Domínguez, A., Primack, J. R., Rosario, D. J., et al. 2011, MNRAS, 410, 2556
- Dwek, E. & Arendt, R. G. 1998, ApJ, 508, L9
- Elbaz, D., Flores, H., Chailan, P., et al. 2002, A&A, 381, L1
- Fazio, G. G., Ashby, M. L. N., Barmby, P., & et al. 2004, ApJS, 154, 39
- Fernandez, E. R., Komatsu, E., Iliev, I. T., & Shapiro, P. R. 2010, ApJ, 710, 1089
- Finkbeiner, D. P., Davis, M., & Schlegel, D. J. 2000, ApJ, 544, 81
- Finke, J. D., Razzaque, S., & Dermer, C. D. 2010, ApJ, 712, 238
- Fomin, V. P., Stepanian, A. A., Lamb, R. C., et al. 1994, Astroparticle Physics, 2, 137
- Franceschini, A., Rodighiero, G., & Vaccari, M. 2008, A&A, 837
- Frayer, D. T., Huynh, M. T., Chary, R., et al. 2006, ApJ, 647, L9
- Gardner, J. P., Brown, T. M., & Ferguson, H. C. 2000, ApJ, 542, L79
- Georgopoulos, M., Finke, J. D., & Reyes, L. C. 2010, ApJ, 714, L157
- Gorjian, V., Wright, E. L., & Chary, R. R. 2000, ApJ, 536, 550
- Gould, R. J. & Schröder, G. P. 1967, Physical Review, 155, 1408
- Hauser, M. G., Arendt, R. G., Kelsall, T., et al. 1998, ApJ, 508, 25

- Kashlinsky, A., Mather, J. C., Odenwald, S., & Hauser, M. G. 1996, *ApJ*, 470, 681
- Keenan, R. C., Barger, A. J., Cowie, L. L., & Wang, W.-H. 2010, *ApJ*, 723, 40
- Kneiske, T. M., Mannheim, K., & Hartmann, D. H. 2002, *A&A*, 386, 1
- Lagache, G., Haffner, L. M., Reynolds, R. J., & Tufte, S. L. 2000, *A&A*, 354, 247
- Levenson, L. R. & Wright, E. L. 2008, *ApJ*, 683, 585
- Levenson, L. R., Wright, E. L., & Johnson, B. D. 2007, *ApJ*, 666, 34
- Li, T. & Ma, Y. 1983, *ApJ*, 317
- Madau, P. & Pozzetti, L. 2000, *MNRAS*, 312, L9
- MAGIC Collaboration, Aleksic, J., Ansoldi, S., et al. 2014, *ArXiv e-prints*
- Mankuzhiyil, N., Persic, M., & Tavecchio, F. 2010, *ApJ*, 715, L16
- Matsumoto, T., Kim, M. G., Pyo, J., & Tsumura, K. 2015, *ArXiv e-prints*
- Matsumoto, T., Matsuura, S., Murakami, H., et al. 2005, *ApJ*, 626, 31
- Matsuoka, Y., Ienaka, N., Kawara, K., & Oyabu, S. 2011, *ApJ*, 736, 119
- Mazin, D. & Raue, M. 2007, *A&A*, 471, 439
- Mazin, D., Tescaro, D., Garczarzyk, M., & et al. 2013, *ArXiv e-prints*
- Metcalfe, L., Kneib, J.-P., McBreen, B., et al. 2003, *A&A*, 407, 791
- Meyer, M., Raue, M., Mazin, D., & Horns, D. 2012, *A&A*, 542, A59
- Orr, M. R., Krennrich, F., & Dwek, E. 2011, *ApJ*, 733, 77
- Papovich, C., Dole, H., Egami, E., et al. 2004, *ApJS*, 154, 70
- Pénin, A., Lagache, G., Noriega-Crespo, A., et al. 2012, *A&A*, 543, A123
- Reinthal, R., Rügamer, S., Lindfors, E. J., et al. 2012, *Journal of Physics Conference Series*, 355, 012017
- Sitarek, J., Gaug, M., Mazin, D., Paoletti, R., & Tescaro, D. 2013, *NIMA*, 723, 109
- Stecker, F. W. & de Jager, O. C. 1996, *Space Science Reviews*, 75, 401
- Stecker, F. W., Malkan, M. A., & Scully, S. T. 2006, *ApJ*, 774
- Tavecchio, F., Maraschi, L., & Ghisellini, G. 1998, *ApJ*, 509, 608
- Thompson, R. I., Eisenstein, D., Fan, X., Rieke, M., & Kennicutt, R. C. 2007, *ApJ*, 657, 669
- Voyer, E. N., Gardner, J. P., Teplitz, H. I., Siana, B. D., & de Mello, D. F. 2011, *ApJ*, 736, 80
- Xu, C. K., Donas, J., Arnouts, S., et al. 2005, *ApJ*, 619, L11
- Zanin, R., Carmona, E., Sitarek, J., & et al. 2013, *Proc of the 33rd ICRC*, Rio de Janeiro, 2
- Zemcov, M., Smidt, J., Arai, T., et al. 2014, *Science*, 346, 732
- <sup>25</sup> now at Centro Brasileiro de Pesquisas Físicas (CBPF), R. Dr. Xavier Sigaud, 150 - Urca, Rio de Janeiro - RJ, 22290-180, Brazil
- <sup>26</sup> now at NASA Goddard Space Flight Center, Greenbelt, MD 20771, USA and Department of Physics and Department of Astronomy, University of Maryland, College Park, MD 20742, USA
- <sup>27</sup> now at Ecole polytechnique fédérale de Lausanne (EPFL), Lausanne, Switzerland
- <sup>28</sup> now at Finnish Centre for Astronomy with ESO (FINCA), Turku, Finland
- <sup>29</sup> also at INAF-Trieste
- <sup>30</sup> also at ISDC - Science Data Center for Astrophysics, 1290, Versoix (Geneva)

- 
- <sup>1</sup> Università di Udine, and INFN Trieste, I-33100 Udine, Italy
- <sup>2</sup> INAF National Institute for Astrophysics, I-00136 Rome, Italy
- <sup>3</sup> Università di Siena, and INFN Pisa, I-53100 Siena, Italy
- <sup>4</sup> Croatian MAGIC Consortium, Rudjer Boskovic Institute, University of Rijeka and University of Split, HR-10000 Zagreb, Croatia
- <sup>5</sup> Max-Planck-Institut für Physik, D-80805 München, Germany
- <sup>6</sup> Universidad Complutense, E-28040 Madrid, Spain
- <sup>7</sup> Inst. de Astrofísica de Canarias, E-38200 La Laguna, Tenerife, Spain
- <sup>8</sup> University of Łódź, PL-90236 Lodz, Poland
- <sup>9</sup> Deutsches Elektronen-Synchrotron (DESY), D-15738 Zeuthen, Germany
- <sup>10</sup> ETH Zurich, CH-8093 Zurich, Switzerland
- <sup>11</sup> IFAE, Campus UAB, E-08193 Bellaterra, Spain
- <sup>12</sup> Universität Würzburg, D-97074 Würzburg, Germany
- <sup>13</sup> Centro de Investigaciones Energéticas, Medioambientales y Tecnológicas, E-28040 Madrid, Spain
- <sup>14</sup> Institute of Space Sciences, E-08193 Barcelona, Spain
- <sup>15</sup> Università di Padova and INFN, I-35131 Padova, Italy
- <sup>16</sup> Technische Universität Dortmund, D-44221 Dortmund, Germany
- <sup>17</sup> Unitat de Física de les Radiacions, Departament de Física, and CERES-IEEC, Universitat Autònoma de Barcelona, E-08193 Bellaterra, Spain
- <sup>18</sup> Universitat de Barcelona, ICC, IEEC-UB, E-08028 Barcelona, Spain
- <sup>19</sup> Japanese MAGIC Consortium, ICRR, The University of Tokyo, Department of Physics and Hakubi Center, Kyoto University, Tokai University, The University of Tokushima, KEK, Japan
- <sup>20</sup> Finnish MAGIC Consortium, Tuorla Observatory, University of Turku and Department of Physics, University of Oulu, Finland
- <sup>21</sup> Inst. for Nucl. Research and Nucl. Energy, BG-1784 Sofia, Bulgaria
- <sup>22</sup> Università di Pisa, and INFN Pisa, I-56126 Pisa, Italy
- <sup>23</sup> ICREA and Institute of Space Sciences, E-08193 Barcelona, Spain
- <sup>24</sup> Università dell'Insubria and INFN Milano Bicocca, Como, I-22100 Como, Italy